The Root Lattice D_4 and Planar Quasilattices with Octagonal and Dodecagonal Symmetry

M. Baake, D. Joseph, and M. Schlottmann
Institut für Theoretische Physik, Universität Tübingen, Auf der Morgenstelle 14, D-7400 Tübingen, Germany

appeared: Int. J. Mod. Phys. **B**, (1991) 1927-1953

PACS numbers: 6150E, 6155H, 6470K, 0220

Abstract

Quasiperiodic patterns with eight- and twelvefold symmetry are presented which share the root lattice D_4, i. e., the 4-D face-centered hypercubic lattice, for their minimal embedding in four-space. We derive the patterns by means of the dualization method and investigate key properties like vertex configurations, local deflation/inflation symmetries and kinematic diffraction. The generalized point symmetries (and thus the Laue group) of these patterns are the dihedral groups d_8 and d_{12}, respectively, which share a common subgroup, d_4. We introduce a continous one-parameter rotation between the two phases which leaves this subgroup invariant. This should prove useful for modelling alloys like $V_{15}Ni_{10}Si$ where quasicrystalline phases with eight- and twelvefold symmetry coexist.

1 Introduction

Since the discovery of decagonal T–phases [1] and other quasiperiodic T–phases with eightfold [2] and twelvefold [3, 4] symmetry, the systematic treatment of planar quasiperiodic patterns has attracted even more attention. On the one hand, they exhibit most of the structural properties of quasiperiodic patterns without suffering from the degenerate situation of 1-D examples like the Fibonacci chain. On the other hand, the rather extensive list of experimental examples [5] shows that these investigations may facilitate the understanding of real 'physical' systems.

The present article is the continuation of the systematic derivation of somehow canonical examples for 2-D and 3-D patterns [6, 7, 8, 9] with non-crystallographic symmetries attached to the standard Fourier modules as classified by algebraic techniques [10]. Here, we will present a unified approach to eight- and twelvefold symmetry. This is possible because minimal (periodic) embedding requires D = 4 in both cases (we have $\phi(8) = \phi(12) = 4$, see Appendix A). Moreover, the 4-D lattices with d_8 or d_{12} (dihedral group) symmetry can be characterized — beyond the lattice constant — by a single parameter each. For certain values of these parameters, we obtain lattices with higher symmetry and can even find an 'intersection point' of these two families: that is the uniquely determined 4-D Bravais lattice of type XXIII/II ([11]), or, in a different language, the root lattice D_4 [12], which is unique due to $D_4^R \cong D_4$.

There are several examples of eight- and twelvefold symmetric quasilattices available in the literature [13] and there are good arguments [8] that not all of them are equivalent — even if they share the same Fourier module. The motivation to add another example stems precisely from the possibility of a simultaneous derivation from the D_4 lattice: this way one may hope to find a structure model for alloys like $V_{15}Ni_{10}Si$ [2, 4] which show both the eightfold and the twelvefold symmetry within the same chemical composition. As will be shown, klotz construction [14] even provides the tools for a transition between the two phases keeping fourfold symmetry and, furthermore, the transition to a periodic cubic phase. This is similar to a procedure proposed in [15] for the transition from icosahedrally symmetric phases to cubic ones.

The paper is organized as follows. In Sec. 2, we start with the 4-D root lattice D_4 and its geometry, i.e., we describe the symmetry, the Voronoi complex and its dual, the Delaunay complex [16] with some emphasis on the hierarchy of the boundaries. This analysis is useful w. r. t. the construction of the quasiperiodic patterns by means of klotz construction. The lattice D_4 is unique in 4-D w. r. t. the possibility to choose 2-D subspaces with either eightfold or twelvefold symmetry which is discussed in Sec. 3. The two reductions are given explicitly together with a continuous rotation between the eight- and the twelvefold cases. In terms of patterns, this transition which always preserves fourfold symmetry is a canonical prototype for a connection between two quasiperiodic phases with different symmetries. The corresponding rotation angle of the so-called Schur rotation [15] has a direct meaning in physical space.

Sec. 4 deals with the eightfold symmetric pattern $\mathcal{T}^{*(8)}_{D_4}$ derived by projection of suitably chosen 2-boundaries of the Delaunay complex. (The second canonical choice, $\mathcal{T}^{(8)}_{D_4}$, stems from 2-boundaries of the Voronoi complex and is briefly discussed in Appendix B.) We present the pattern, some of its key properties (like vertex configurations, deflation/inflation symmetries, and the connection to Beenker's pattern [17]) followed by the Fourier analysis of δ-scatterers on vertex positions. In Sec. 5, the analogous program is outlined for the twelvefold symmetric pattern $\mathcal{T}^{*(12)}_{D_4}$ while its counterpart, $\mathcal{T}^{(12)}_{D_4}$, is deferred to Appendix C. This is followed by some concluding remarks.

2 The 4-D geometry of the root lattice D_4

In four dimensions, there is only one hypercubic centering that is different from the primitive hypercubic lattice, because F–type (generalized face-centered lattice) and I–type (generalized body-centered lattice) are equivalent. We will take the root lattice D_4 as representative, which is generated by the integer linear combinations of the four vectors

$$\mathbf{e}_1-\mathbf{e}_2,\qquad \mathbf{e}_2-\mathbf{e}_3,\qquad \mathbf{e}_3-\mathbf{e}_4,\qquad \mathbf{e}_3+\mathbf{e}_4, \tag{2.1}$$

where the $\mathbf{e}_i$ denote the standard Euclidean basis in $\mathbb{R}^4$. The vectors $2\mathbf{e}_1,\ldots,2\mathbf{e}_4$ generate a primitive sublattice of minimal lattice constant.

The lattice D_4 possesses 24 Voronoi vectors $\pm(\mathbf{e}_i \pm \mathbf{e}_j), i \neq j$, and provides the densest lattice packing in 4-D — the so-called kissing number is 24 (for details see [12]). The holohedry H of D_4 is larger than the hypercubic group $\Omega(4)$ [18], namely

$$H = \Omega^+(4) \otimes_s S_3 \tag{2.2}$$

where $\Omega^+(4)$ is the subgroup of $\Omega(4)$ with even sign flips and S_3 is generated by the cyclic operation $(\mathbf{e}_1-\mathbf{e}_2) \to (\mathbf{e}_3-\mathbf{e}_4) \to (\mathbf{e}_3+\mathbf{e}_4) \to (\mathbf{e}_1-\mathbf{e}_2)$ and the reflection $\mathbf{e}_4 \to -\mathbf{e}_4$. The latter transformation completes $\Omega^+(4)$ to $\Omega(4)$ which thus is a subgroup of H of index 3, $[H : \Omega(4)] = 3$. H is the holohedry 33/16 of [11]. The character table can be found in [19] together with a (non-minimal) set of generators.

We will now describe the geometry of the Voronoi cell $V(\mathbf{0})$,

$$V(\mathbf{0}) := \{\mathbf{x} \in \mathbb{R}^4 \ \mid\ |\mathbf{x}| \leq |\mathbf{x}-\mathbf{q}| \text{ for all } \mathbf{q} \in D_4\} \tag{2.3}$$

which is the closure of a fundamental domain of the lattice. $V(\mathbf{0})$ can be given as the convex hull of its vertices which are the 24 points $(\pm1,0,0,0)$ and $((\pm1,\pm1,\pm1,\pm1)/2)$ together with their permutations, given in the standard Euclidean basis, i.e.,

$$V(\mathbf{0}) := \mathrm{conv}\{\pi(\pm 1,0,0,0),\ \frac{1}{2}\sigma(\pm 1,\ldots,\pm 1)\ \mid\ \pi,\sigma \in S_4\} \tag{2.4}$$

This object turns out to be the regular 4-D polytope $\{3,4,3\}$ with 24 vertices, 96 edges, 96 2-D faces and 24 hypersurfaces [20]. Let us define the hyperplanes

$$H^0_{\mathbf{v}} = \{\mathbf{x} \in \mathbb{R}^4\ \mid\ |\mathbf{x}|^2 = |\mathbf{x}-\mathbf{v}|^2\}. \tag{2.5}$$

If $\mathbf{v}$ is a Voronoi vector, one has $|\mathbf{v}|^2 = 2$ and, e.g.,

$$H^0_{\mathbf{e}_1+\mathbf{e}_2} = \{\mathbf{x} \in \mathbb{R}^4\ \mid\ \mathbf{x}\cdot(\mathbf{e}_1+\mathbf{e}_2) = 1\} \tag{2.6}$$

Now, the 3-boundaries of $V(\mathbf{0})$ are the 24 octahedra obtained as

$$\begin{aligned} P = V(\mathbf{0}) \cap H^0_{\mathbf{e}_1+\mathbf{e}_2} &= \{\mathbf{x} \in V(\mathbf{0})\ \mid\ \mathbf{x}\cdot(\mathbf{e}_1+\mathbf{e}_2) = 1\} \\ &= \mathrm{conv}\{\mathbf{e}_1, \mathbf{e}_2, \frac{1}{2}(1,1,\pm 1,\pm 1)\} \end{aligned} \tag{2.7}$$

(and similarly for the other Voronoi vectors) while its dual boundary is the line spanned by the Voronoi vector $\mathbf{e}_1+\mathbf{e}_2$,

$$P^* = \{\mu(\mathbf{e}_1+\mathbf{e}_2)\ \mid\ 0 \le \mu \le 1\}. \tag{2.8}$$

These 24 objects form a single orbit w. r. t. the holohedry H as do the 96 2-boundaries like

$$P = V(\mathbf{0}) \cap H^0_{\mathbf{e}_1+\mathbf{e}_2} \cap H^0_{\mathbf{e}_2+\mathbf{e}_3} = \mathrm{conv}\{\mathbf{e}_2, \frac{1}{2}(1,1,1,\pm 1)\}. \tag{2.9}$$

They are regular triangles like their dual objects, e.g.,

$$P^* = \{\mu_1(\mathbf{e}_1+\mathbf{e}_2) + \mu_2(\mathbf{e}_2+\mathbf{e}_3)\ \mid\ \mu_i \ge 0, \mu_1+\mu_2 \le 1\}. \tag{2.10}$$

Again, they are combined to a single H-orbit. This is a consequence of $V(\mathbf{0})$ being the regular polytope $\{3,4,3\}$ wherefore all boundaries of the same dimension lie in a single orbit of the symmetry group of $\{3,4,3\}$ which is isomorphic with H.

Now, the 1-boundaries of $V(\mathbf{0})$ are either described by

$$P = V(\mathbf{0}) \cap H^0_{\mathbf{e}_1+\mathbf{e}_2} \cap H^0_{\mathbf{e}_2+\mathbf{e}_3} \cap H^0_{\mathbf{e}_1+\mathbf{e}_3} = \mathrm{conv}\{\frac{1}{2}(1,1,1,\pm 1)\} \tag{2.11}$$

with the dual 3-D object

$$P^* = \{\mu_1(\mathbf{e}_1+\mathbf{e}_2) + \mu_2(\mathbf{e}_2+\mathbf{e}_3) + \mu_3(\mathbf{e}_1+\mathbf{e}_3)\ \mid\ \mu_i \ge 0, \mu_1+\mu_2+\mu_3 \le 1\}. \tag{2.12}$$

or by

$$P = V(\mathbf{0}) \cap H^0_{\mathbf{e}_1+\mathbf{e}_2} \cap H^0_{\mathbf{e}_1+\mathbf{e}_3} \cap H^0_{\mathbf{e}_1+\mathbf{e}_4} = \mathrm{conv}\{\mathbf{e}_1, \frac{1}{2}(1,1,1,1)\} \tag{2.13}$$

with the dual 3-boundary

$$P^* = \{\mu_1(\mathbf{e}_1+\mathbf{e}_2) + \mu_2(\mathbf{e}_1+\mathbf{e}_3) + \mu_3(\mathbf{e}_1+\mathbf{e}_4)\ \mid\ \mu_i \ge 0, \mu_1+\mu_2+\mu_3 \le 1\}, \tag{2.14}$$

96 pieces alltogether, the dual 3-boundaries being regular tetrahedra.

The vertices of $V(\mathbf{0})$ have been given already, their dual objects — the Delaunay cells of D_4 — are regular 4-D polytopes of type $\{3,3,4\}$ with symmetry group $\Omega(4)$, e.g., for $P = \{\frac{1}{2}(1,1,1,1)\}$ one obtains

$$P^* = \mathrm{conv}\{0, \mathbf{e}_1+\mathbf{e}_2+\mathbf{e}_3+\mathbf{e}_4, \mathbf{e}_i+\mathbf{e}_j\ \mid\ i<j\}. \tag{2.15}$$

Of primary importance for our purposes are the 2-boundaries and their duals because they serve as preimages of the tiles of the patterns to be constructed. No matter which version we choose — projection of Delaunay objects or Voronoi objects into the 2-D 'physical' space — we will end up with triangles only, the shape of which depends on the projection space chosen. This will be explained in the following Section.

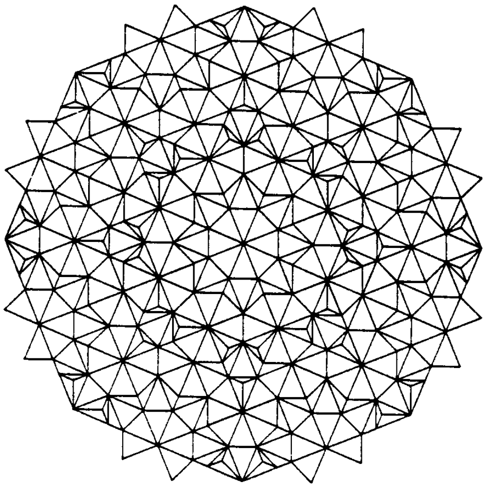

Figure 1: Eightfold symmetric pattern $\mathcal{T}^{*(8)}_{D_4}$. The tiles are projection images of Delaunay 2-boundaries. It is an example for a quasiperiodic pattern during "Schur rotation" (rotation parameter $\phi = 0$) with higher symmetry.

3 2-D subspaces with eight- and twelvefold symmetries

The canonical 4-D representation T of H is irreducible [18], i.e., it does not allow nontrivial invariant subspaces. However, several subgroups of H do, especially the groups $d_8 = \langle\langle \mathbf{g}_8, \mathbf{s}\rangle\rangle$ and $d_{12} = \langle\langle \mathbf{g}_{12}, \mathbf{s}\rangle\rangle$ where

$$T(\mathbf{g}_8) := \begin{pmatrix} 0 & 0 & 0 & -1 \\ 1 & 0 & 0 & 0 \\ 0 & 1 & 0 & 0 \\ 0 & 0 & 1 & 0 \end{pmatrix}, \quad T(\mathbf{g}_{12}) := \frac{1}{2}\begin{pmatrix} -1 & 1 & -1 & -1 \\ 1 & 1 & 1 & -1 \\ 1 & 1 & -1 & 1 \\ -1 & 1 & 1 & 1 \end{pmatrix}, \tag{3.1}$$

and

$$T(\mathbf{s}) := \begin{pmatrix} 1 & 0 & 0 & 0 \\ 0 & 0 & 0 & -1 \\ 0 & 0 & -1 & 0 \\ 0 & -1 & 0 & 0 \end{pmatrix}, \tag{3.2}$$

These two groups possess a common subgroup, $d_4 = \langle\langle \mathbf{g}_4, \mathbf{s}\rangle\rangle$ with $\mathbf{g}_4 = \mathbf{g}_8^2 = \mathbf{g}_{12}^3$ that plays an important role in the description of a continuous transition between an eightfold and a twelvefold symmetric pattern. But let us focus on the single patterns first.

The representation T, restricted to the subgroup d_8, decomposes into two inequivalent irreducible 2-D representations according to

$$U_8\, T(\mathbf{g})\, U_8^{-1} = T^{red}(\mathbf{g}), \qquad (\mathbf{g} \in d_8), \tag{3.3}$$

where

$$U_8 := \sqrt{\frac{1}{2}}\begin{pmatrix} 1 & \sqrt{\frac{1}{2}} & 0 & -\sqrt{\frac{1}{2}} \\ 0 & \sqrt{\frac{1}{2}} & 1 & \sqrt{\frac{1}{2}} \\ 1 & -\sqrt{\frac{1}{2}} & 0 & \sqrt{\frac{1}{2}} \\ 0 & -\sqrt{\frac{1}{2}} & 1 & -\sqrt{\frac{1}{2}} \end{pmatrix}, \tag{3.4}$$

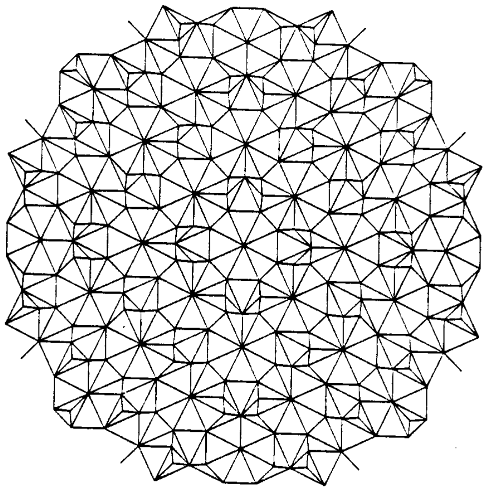

Figure 2: Generic example for a quasiperiodic, fourfold symmetric pattern during “Schur rotation” (rotation parameter $\phi = \pi/24$).

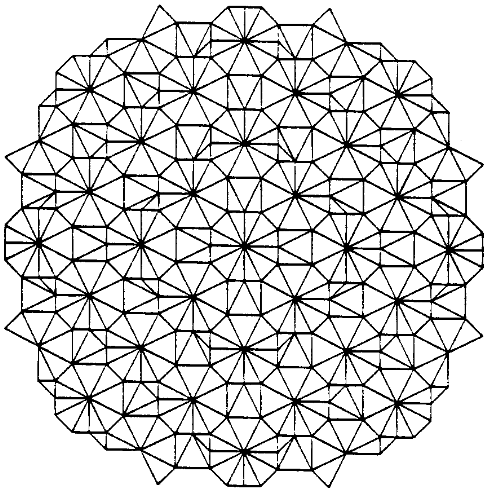

Figure 3: Generic example for a quasiperiodic, fourfold symmetric pattern during “Schur rotation” (rotation parameter $\phi = \pi/18$).

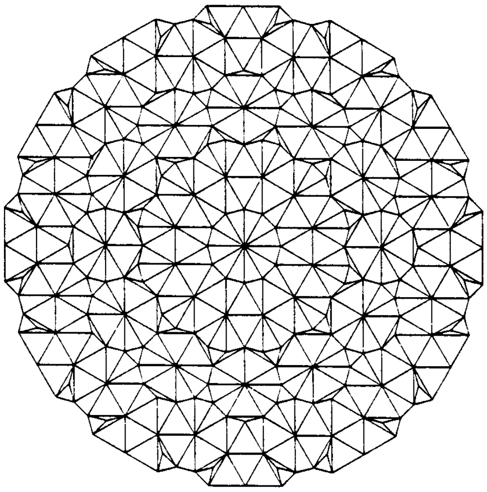

Figure 4: Twelvefold symmetric pattern $\mathcal{T}^{*(12)}_{D_4}$. The tiles are projection images of Delaunay 2-boundaries. It is an example for a quasiperiodic pattern during "Schur rotation" (rotation parameter $\phi = \arccos((\sqrt{3+\sqrt{3}} + \sqrt{3-\sqrt{3}})/(2\sqrt{3})) \approx 17.6^0$) with higher symmetry.

and

$$T^{red}(\mathbf{g}_8) := \begin{pmatrix} c & -s & 0 & 0 \\ s & c & 0 & 0 \\ 0 & 0 & c' & -s' \\ 0 & 0 & s' & c' \end{pmatrix}, \qquad T^{red}(\mathbf{s}) := diag\ (1,-1,1,-1), \tag{3.5}$$

with

$$\begin{aligned} c := \cos(\delta),\ s := \sin(\delta), \\ c' := \cos(5\delta),\ s' := \sin(5\delta), \end{aligned} \tag{3.6}$$

($\delta := \frac{2\pi}{8}$). The two invariant subspaces are identified with the physical space $\mathbb{E}_{\parallel}$ and the perpendicular space $\mathbb{E}_{\perp}$, respectively. The eightfold rotation appears as an unusual rotation around $5 \cdot \frac{2\pi}{8}$ in perpendicular space instead of $3 \cdot \frac{2\pi}{8}$. This does not affect the pattern at all, but facilitates the unified description of the eightfold and the twelvefold symmetry to be described later on because of $5 \equiv 1(\mathrm{mod} 4)$.

Similarly, in the case of d_{12}, we find the decomposition

$$U_{12}\, T(\mathbf{g})\, U_{12}^{-1} \ = T^{red}(\mathbf{g}), \qquad \mathbf{g} \in d_{12}, \tag{3.7}$$

with

$$U_{12} := \sqrt{\frac{1}{1+\alpha^2}} \begin{pmatrix} 1 & \frac{\alpha}{\sqrt{2}} & 0 & -\frac{\alpha}{\sqrt{2}} \\ 0 & \frac{\alpha}{\sqrt{2}} & 1 & \frac{\alpha}{\sqrt{2}} \\ \alpha & -\frac{1}{\sqrt{2}} & 0 & \frac{1}{\sqrt{2}} \\ 0 & -\frac{1}{\sqrt{2}} & \alpha & -\frac{1}{\sqrt{2}} \end{pmatrix}, \qquad (\alpha := 2\cos(\frac{\pi}{12})) \tag{3.8}$$

and

$$T^{red}(\mathbf{g}_{12}) := \begin{pmatrix} c & -s & 0 & 0 \\ s & c & 0 & 0 \\ 0 & 0 & c' & -s' \\ 0 & 0 & s' & c' \end{pmatrix}, \qquad T^{red}(\mathbf{s}) := diag(1,-1,1,-1), \tag{3.9}$$

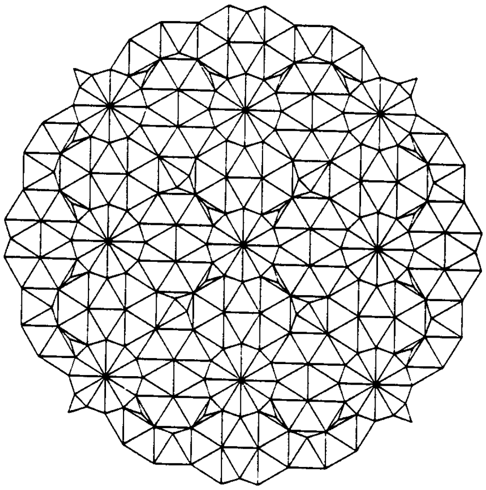

Figure 5: Generic example for a quasiperiodic, fourfold symmetric pattern during “Schur rotation” (rotation parameter $\phi = \pi/9$).

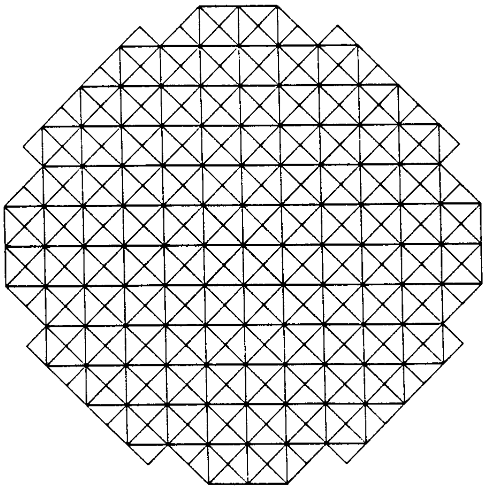

Figure 6: Generic example for a periodic, fourfold symmetric pattern during “Schur rotation” (rotation parameter $\phi = \pi/4$).

with

$$
\begin{aligned}
c &:= \cos(\beta),\ s := \sin(\beta), \\
c' &:= \cos(5\beta),\ s' := \sin(5\beta),
\end{aligned}
\tag{3.10}
$$

where $\beta := \frac{2\pi}{12}$. Again, the two irreps are inequivalent which is no longer true if we restrict T to the common subgroup d_4, where they are identical.

In the case of d_{12} the projection image of the Euclidean basis vectors $\mathbf{e}_1, \ldots, \mathbf{e}_4$ seems to be more complicated because $\mathbf{e}_1$ and $\mathbf{e}_2$ lie in two different d_{12} orbits, but there is no real difficulty connected with it. On the contrary, in this formulation we can find a unified reduction that depends on one parameter ϕ. Since

$$
T^{red}(\mathbf{g}_4^k) := \mathbb{1} \otimes \begin{pmatrix} \cos(\theta) & -\sin(\theta) \\ \sin(\theta) & \cos(\theta) \end{pmatrix}, \text{ and } \quad T^{red}(\mathbf{s}) := \mathbb{1} \otimes \begin{pmatrix} 1 & 0 \\ 0 & -1 \end{pmatrix}, \tag{3.11}
$$

with $\theta = k\pi/2$, the irreps in $\mathbb{E}_\parallel$ and $\mathbb{E}_\perp$ are identical for the subgroup d_4. We thus have a phase freedom [15] according to Schur's lemma, i.e.,

$$
[T^{red}(\mathbf{g}), R(\phi)] = 0, \mathbf{g} \in d_4, \text{ with } \quad R(\phi) := \begin{pmatrix} \cos(\phi) & -\sin(\phi) \\ \sin(\phi) & \cos(\phi) \end{pmatrix} \otimes \mathbb{1}. \tag{3.12}
$$

If we take the ansatz

$$
U(\phi) = R(\phi) \cdot U_8, \tag{3.13}
$$

we will find the well-known cases

$$
U(0) = U_8, \quad U(\phi') = U_{12}, \quad \phi' = \arccos\left(\frac{\sqrt{3+\sqrt{3}} + \sqrt{3-\sqrt{3}}}{2\sqrt{3}}\right) \approx 17.6^0 \tag{3.14}
$$

but continuously many points in between and beyond, all of them with d_4 symmetry. One can easily see that nothing new happens outside the interval $[0, \pi/2]$ for ϕ, $\phi = \pi/2$ being case of a periodic projection.

As shown in Eq. 3.12, the 4-D rotation $R(\phi)$ leaves the common subgroup d_4 invariant. For every chosen ϕ we will get different subspaces $\mathbb{E}_\parallel(\phi)$ and $\mathbb{E}_\perp(\phi)$ where we can perform the klotz construction. This technique is sketched in Sec. 4 and gives rise to an explicit tile-by-tile algorithm based on the dualization scheme. It is based on the windows in $\mathbb{E}_\perp$ which here are either the projected Voronoi cells or the projected Delaunay cells. The algorithm has been described in detail in two earlier publications [6, 21]. It leads to a family of different tilings, $\mathcal{T}_{D_4}^{(\phi)}, \mathcal{T}_{D_4}^{*(\phi)}$, which all preserve fourfold symmetry as do the corresponding windows in $\mathbb{E}_\perp$. Figs. 1-5 show some quasiperiodic examples obtained this way. In Fig. 1 and Fig. 4, the eightfold and the twelvefold symmetric patterns are presented, which will be described in Sec. 4 and Sec. 5, respectively. There exists a dense set of ϕ's for which $\mathbb{E}_\parallel(\phi)$ contains a 2-D netplane of the D_4 lattice. As a consequence, the corresponding tilings are periodic. Fig. 6 shows, as an example, the tiling with $\phi = \pi/4$, which is the periodic tiling of minimal period.

As mentioned in the introduction, this unified description of an octagonal and a dodecagonal quasilattice might prove useful for the structure models of alloys like $V_{15}Ni_{10}Si$ which can show both symmetries in samples of the same chemical composition [2, 4]. The rotation angle ϕ gives rise to an order parameter $\eta(\phi)$ in $\mathbb{E}_\parallel$ which turns out to be

$$
\eta(\phi) = \frac{\mid \pi_\parallel(\mathbf{e_1}) \mid}{\mid \pi_\parallel(\mathbf{e_2}) \mid} = \frac{\mid \cos(\phi) - \sin(\phi) \mid}{\mid \cos(\phi) + \sin(\phi) \mid}. \tag{3.15}
$$

Precisely the same mechanism can be applied to the octagonal pattern based on $\mathbb{Z}^4$ [17, 21] in order to describe a transition from the quasiperiodic eightfold phase to a periodic one maintaining fourfold symmetry. This has been observed experimentally [22] in electron microscopy of NiCrSi.

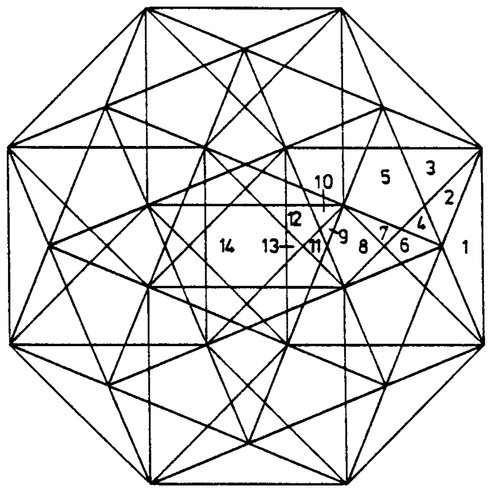

Figure 7: Projection image of the Voronoi cell of D_4 in $\mathbb{E}_\perp$ with eightfold symmetry. The numbering of the elementary polygons corresponds to the numbering of vertex configurations in Fig. 8.

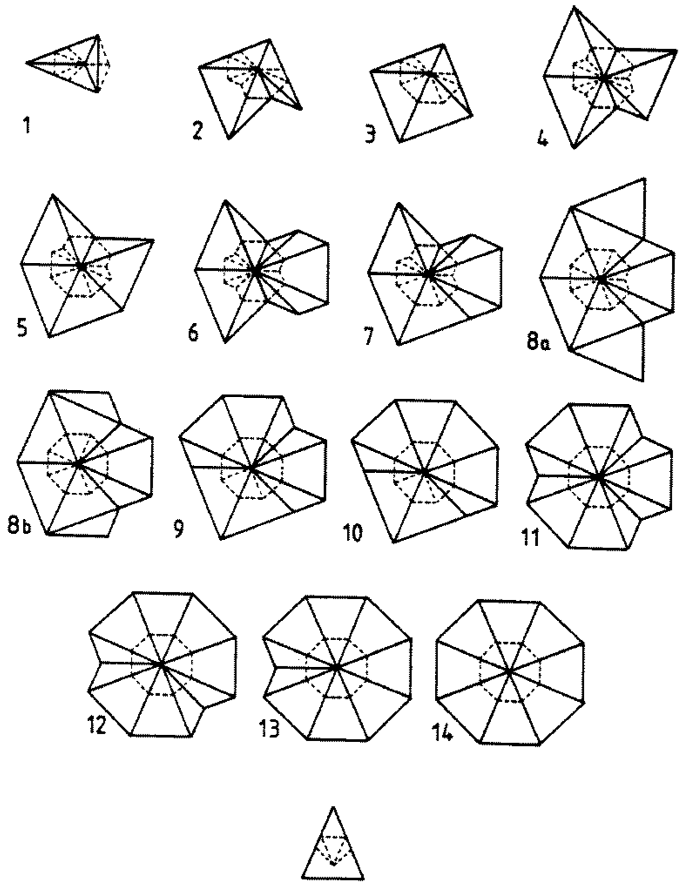

Figure 8: Vertex configurations of $\mathcal{T}^{*(8)}_{D_4}$ and their deflation. The non-uniquely deflated vertex 8 appears in two variations; their deflation is controlled by the immediate neighbourhood. The single triangle at the bottom of the picture indicates the deflation rule of its pentagon-shaped centre.

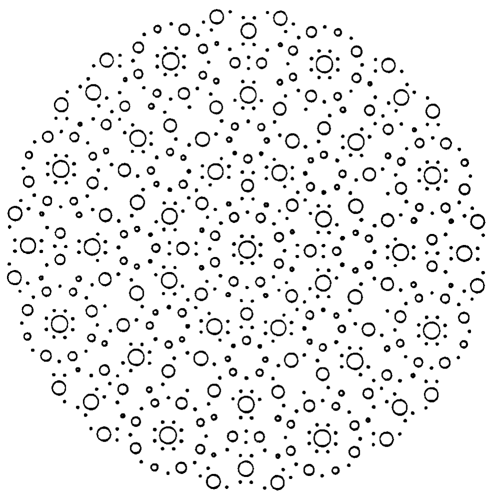

Figure 9: Calculated diffraction image of delta scatterers at vertex positions of $\mathcal{T}^{*(8)}_{D_4}$.

4 A quasiperiodic pattern with eightfold symmetry

Let us now describe the pattern $\mathcal{T}^{*(8)}_{D_4}$ that is obtained by klotz construction where the preimages of the tiles are 2-boundaries of the Delaunay complex. The second canonical choice, where the 2-boundaries of the Voronoi complex are to be projected onto the physical space $\mathbb{E}_{\|}$, is called $\mathcal{T}^{(8)}_{D_4}$ and briefly described in Appendix B.

The dualization leads to the following recipe for the pattern desired. Take the physical space $\mathbb{E}_{\|}$, which in this case is a 2-D hyperplane, and a generic shift vector $\mathbf{c}_{\perp}$. Now, for every 2-boundary P of the Voronoi complex of D_4 that has an intersection with $\mathbf{c}_{\perp} + \mathbb{E}_{\|}$, project its dual 2-boundary P^* down to $\mathbb{E}_{\|}$. This procedure gives an infinite pattern with generalized eightfold symmetry, cf. Fig. 1, that is built from three types of triangles.

Algebraically, it can be defined as follows

$$\mathcal{T}^{*(8)}_{D_4}(\mathbf{c}_{\perp}) = \{\pi_{\|}(P^*) \ | \ P \in \mathcal{V}^{(2)}, \quad \mathbf{c}_{\perp} \in \pi_{\perp}(P)\} \tag{4.1}$$

where $\mathcal{V}^{(2)} = \{P \in \mathcal{V} \ | \ \dim(P) = 2\}$ denotes the 2-skeleton of the Voronoi complex $\mathcal{V} = \{P \ | \ P$ is a boundary of $V(\mathbf{q}), \mathbf{q} \in D_4\}$. From this algebraic description a very effective construction algorithm can be derived which generates the pattern tile by tile. For more details on this systematic approach the reader is referred to an earlier publication [6] where this technique has thoroughly been outlined. Let us only remark that the choice of $\mathbf{c}_{\perp}$ contains some subtleties, i.e., for the generic, non-singular case $\mathbf{c}_{\perp}$ must be selected in such a way that it is not contained in the projection image of any boundary of dimension less than two. Since this only excludes a set of measure zero we will not spend more effort on it here.

The pattern obtained from generic $\mathbf{c}_{\perp}$ belongs to a single local isomorphism class. Let us now, in an illustrative way, describe some of its properties. For a given $\mathbf{c}_{\perp}$, the set of vertices of the pattern $\mathcal{T}^{*(8)}_{D_4}(\mathbf{c}_{\perp})$ takes the form

$$\{\pi_{\|}(\mathbf{q}) \ | \ \mathbf{q} \in D_4, \quad \mathbf{c}_{\perp} - \pi_{\perp}(\mathbf{q}) \in \pi_{\perp}(V(\mathbf{0}))\} \tag{4.2}$$

while the complete vertex configuration around a vertex point $\pi_{\|}(\mathbf{q})$ can be written down as

$$\{\pi_{\|}(P^*) + \pi_{\|}(\mathbf{q}) \ | \ P \in \mathcal{V}^{(2)}, \quad P \subseteq V(\mathbf{0}), \quad \mathbf{c}_{\perp} - \pi_{\perp}(\mathbf{q}) \in \pi_{\|}(P)\} \tag{4.3}$$

The restriction of $\mathbf{c}_{\perp}$ to the generic case guarantees a common overlap of all $\pi_{\perp}(P)$, the corresponding $\pi_{\|}(P^*) + \pi_{\|}(\mathbf{q})$ of which belong to the same configuration around $\pi_{\|}(\mathbf{q})$. Consequently,

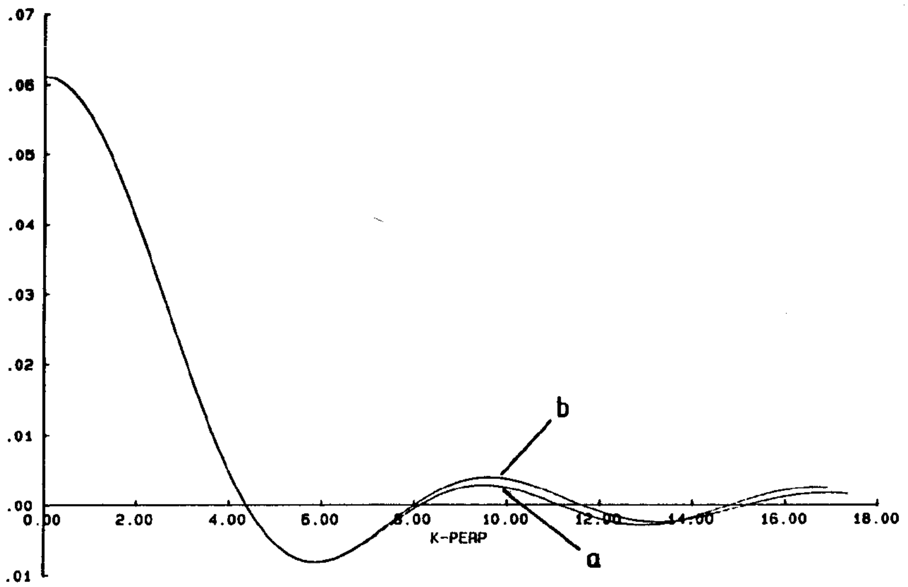

Figure 10: Comparison of the kinematical factor for $\mathbf{k}_\perp$ in $\mathbf{e}_1$-direction calculated a) exactly and b) by sphere approximation.

there is a one-to-one correspondence between complete vertex configurations in $\mathbb{E}_\parallel$ and maximal common overlaps of projection images of 2-boundaries of $V(\mathbf{0})$ in $\mathbb{E}_\perp$. The latter can be visualized immediately inside the projection image $\pi_\perp(V(\mathbf{0}))$ of the Voronoi cell, cf. Fig. 7, which is subdivided into so-called elementary polygons. A representative set of them w. r. t. the generalized point symmetry d_8 is labelled by the numbers $1, \ldots, 14$ which simultaneously refers to the 14 possible vertex configurations shown in Fig. 8.

The space $\mathbb{E}_\parallel$ is not contained in any net plane of the lattice D_4 wherefore the projection images of the lattice points are dense in $\mathbb{E}_\perp$ and, moreover, uniformly distributed. Consequently, $\{\mathbf{c}_\perp - \pi_\perp(\mathbf{q}) \mid \mathbf{q} \in D_4\} \cap \pi_\perp(V(\mathbf{0}))$ lies densely in $\pi_\perp(V(\mathbf{0}))$ and is uniformly distributed there — so exactly the fraction $area(\mathcal{E})/area(\pi_\perp(V(\mathbf{0}))$ of all the vertices of $\mathcal{T}^{*(8)}_{D_4}(\mathbf{c}_\perp)$ are from the class represented by the elementary polygon $\mathcal{E}$. The areas of the representative elementary polygons are easy to determine, the resulting frequencies ν of the corresponding vertex configuration classes are listed in Tab. 1, where we have added up all contributions from the complete d_8 orbits.

Let us now turn to the deflation/inflation symmetry of the eightfold pattern. There exists a linear transformation in the 4-D hyperspace which leaves the D_4 lattice invariant and acts on $\mathbb{E}_\parallel$ and $\mathbb{E}_\perp$ seperately as a contraction and dilation, respectively,

$$M = \frac{1}{\lambda} \cdot \pi_\parallel + (-\lambda) \cdot \pi_\perp \tag{4.4}$$

where $\lambda = 1 + \sqrt{2}$ is the so-called silver number [23].

Formally, M acts on the derived 2-D pattern by transforming $\mathcal{T}(\mathbf{c}_\perp)$ into $\frac{1}{\lambda}\mathcal{T}(-\frac{1}{\lambda}\mathbf{c}_\perp)$. It turns out that this transformation can be described in a completely local way, i.e., it is possible to determine the tiles at some place in $\frac{1}{\lambda}\mathcal{T}(-\frac{1}{\lambda}\mathbf{c}_\perp)$ only with the knowledge of the neighbourhood in $\mathcal{T}(\mathbf{c}_\perp)$ up to a certain radius. In other words, M provides a local deflation transformation of our pattern. This local deflation works as a description for the transformation of the vertex configurations as follows:

If $\pi_\parallel(\mathbf{q})$ is a vertex point of the tiling $\mathcal{T}(\mathbf{c}_\perp)$, then it is a vertex point of $\mathcal{T}(\mathbf{c}_\perp) = \frac{1}{\lambda}\mathcal{T}(-\frac{1}{\lambda}c_\perp)$, and the vertex configuration around $\pi_\parallel(\mathbf{q})$ is just the configuration, rescaled by a factor of $\frac{1}{\lambda}$, which is represented by the elementary polygon that contains $-\frac{1}{\lambda}(\mathbf{c}_\perp - \pi_\parallel(\mathbf{q}))$. A look at the decomposition of $\pi_\perp(V(\mathbf{0}))$ into elementary polygons (Fig. 7) leads to the simple rules indicated in Fig. 8. Almost every vertex configuration is unambiguously transformed under deflation, except for type 8. A more detailed investigation shows that configurations of type 8 must be accompanied by two 'wings' on their long sides (cf. Fig. 8). Depending on the composition of these two wings one can decide which deflation possibility is to be chosen. Applying these vertex deflations on the pattern will leave holes inside the big isosceles triangles. These holes must be filled with a deflated big isosceles triangle in upside down orientation (cf. Fig. 8).

Looking at the dissection of the single tiles these rules will result in a unique dissection of the small isosceles triangle and the irregular one whereas the big isosceles triangle is dissected in four different ways.

Let us mention that an inspection of the construction algorithm shows that there exists also a local inflation of the pattern, but we will leave out the details here.

At this point, we would like to comment on the Fourier properties of this pattern with eightfold symmetry. The Laue group, i.e., the symmetry group of a characteristic diffraction plot, will coincide with d_8, the generalized point symmetry of $\mathcal{T}^{*(8)}_{D_4}$. To describe the Fourier transform, we need a k-space $\widetilde{\mathbb{E}}^4$, split as before: $\widetilde{\mathbb{E}}^4 = \widetilde{\mathbb{E}_\parallel} + \widetilde{\mathbb{E}_\perp}$, together with the lattice $2\pi \cdot D_4^R$ which is spanned by

$$\mathbf{k}_1^R = 2\pi \mathbf{e}_1, \quad \mathbf{k}_2^R = 2\pi(\mathbf{e}_1 + \mathbf{e}_2), \quad \mathbf{k}_3^R = 2\pi \frac{1}{2}(\mathbf{e}_1 + \mathbf{e}_2 + \mathbf{e}_3 - \mathbf{e}_4), \quad \mathbf{k}_4^R = 2\pi \frac{1}{2} \sum_{j=1}^{4} \mathbf{e}_i \tag{4.5}$$

The lattice points then are $\mathbf{k}^R = \sum_i h_i \mathbf{k}_i^R$ with $h_i \in \mathbb{Z}$ wherefore the h_i's are called generalized Miller indices. For an explicit application one probably would choose a different basis for practical reasons, but this does not matter in our context.

In the quasicrystal model [24], which we will focus on for the sake of simplicity, the three tiles serve as cells and carry fixed densities in $\mathbb{E}_\parallel$. It is not difficult to generalize this situation but this is not necessary for our present needs, because we will not go beyond an illustrative demonstration of the Fourier transform of delta scatterers on vertex positions. For a systematic approach on the klotz construction we refer to [14], here we will only give the somewhat simpler formula for the Fourier transform of the vertex decoration, i.e., of delta scatterers of equal strength on each vertex point of the generic pattern $\mathcal{T}^{*(8)}_{D_4}(\mathbf{c}_\perp)$. The density distributions then reads

$$f(\mathbf{x}_\parallel) = \sum_{\mathbf{q}_\parallel \in \mathcal{T}^{*(8)}_{D_4}} \delta(\mathbf{x}_\parallel - \mathbf{q}_\parallel) \tag{4.6}$$

and we obtain the Fourier transform

$$\tilde{f}(\mathbf{k}_\parallel) = \frac{1}{\mathrm{vol(FD)}} \sum_{\mathbf{k}^R \in 2\pi D_4^R} \delta(\mathbf{k}_\parallel - {\mathbf{q}_\parallel}^R) \cdot S(\mathbf{k}_\parallel) \cdot K({\mathbf{k}_\perp}^R) \tag{4.7}$$

where vol(FD) $= 2$ is the volume of the fundamental domain $V(\mathbf{0})$ of D_4, K denotes the kinematic factor

$$K({\mathbf{k}_\parallel}^R) = \exp(i{\mathbf{k}_\perp}^R \cdot \mathbf{c}_\perp) \cdot \int_{\pi_\perp(V(0))} \exp(-i{\mathbf{k}_\perp}^R \cdot \mathbf{x}_\perp) d^2\mathbf{x}_\perp, \tag{4.8}$$

while S, the structure factor, reduces to $S(\mathbf{k}_\parallel) \equiv 1$ in this situation.

The result is shown in Fig. 9, where the exact integration over $\pi_\perp(V(\mathbf{0}))$ — which is a regular octagon of area λ — has been used for the kinematic factor. An approximation of the regular octagon by a circle of radius $\sqrt{\pi/\lambda}$ would do as well, the deviations are typically in the region of 10^{-4} w. r. t. the central peak. In this case, the kinematic factor can be expressed by means of the Bessel function:

$$K({\mathbf{k}_\perp}^R) = \exp(i{\mathbf{k}_\perp}^R \cdot \mathbf{c}_\perp) \frac{2\pi r}{|{\mathbf{k}_\perp}^R|} \cdot J_1(|{\mathbf{k}_\perp}^R|\, r). \tag{4.9}$$

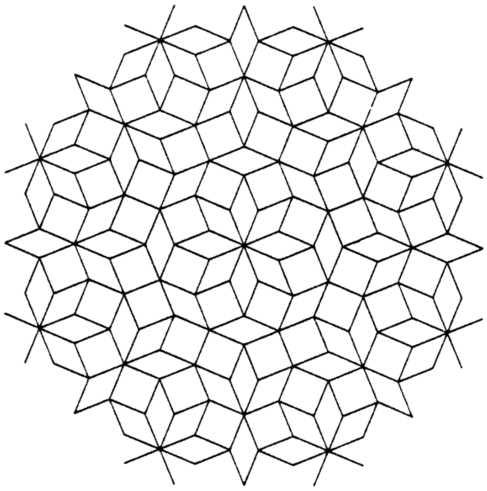

Figure 11: Beenker's pattern as derived from $\mathbb{Z}^4$, scaled by $\sqrt{1+\lambda}$ and rotated by $\pi/8$

On the other hand, in precise terms, the circle approximation corresponds to a different pattern of point scatterers that certainly does not fit into the tiling of Fig. 1. This shows that the significant information on the real space structure is encoded in the intensities of the small and very small peaks — the big ones carry only the coarse kinematic structure, (cf. Fig. 10).

Let us, at this point, comment on the relation to the well-known Beenker pattern $\mathcal{T}^*_{\mathbb{Z}_4}$ which can be derived from the 4-D primitive hypercubic lattice $\mathbb{Z}^4$ [17, 21]. Both $\pi_\|(\mathbb{Z}^4)$ and $\pi_\|(D_4)$ yield eightfold symmetric modules in the plane $\mathbb{E}_\|$ which must be isomorphic [10]. Indeed, a rotation by $\pi/8$ and subsequent dilation by $\sqrt{1+\lambda}$ will bring $\pi_\|(\mathbb{Z}^4)$ to $\pi_\|(D_4)$. If we apply the corresponding transformation to the pattern itself, we obtain Fig. 11 which can be put immediately onto Fig. 1 to visualize the local transformation rules to pass from $\mathcal{T}^{*(8)}_{D_4}$ to $\mathcal{T}^*_{\mathbb{Z}^4}$: a) erase vertex No. 1, b) erase all original and newly produced vertices of type 3, c) erase the intersection lines of all triangles which lie outside the arising squares. This means that the latter is locally derivable [8] from the former. A detailed look at the Voronoi cells, or, more precisely, their projections to $\mathbb{E}_\perp$, shows that the converse is not possible because not all elementary polygons inside $\pi_\perp(V_{D_4}(\mathbf{0}))$ — which are the 'windows' of the vertex configurations — can be obtained from finite intersections of projected boundaries of $\mathbb{Z}^4$. Therefore, we consider the patterns as representatives of different tiling classes [8] that nevertheless share the same Fourier module.

5 A quasiperiodic pattern with twelvefold symmetry

Having presented the eightfold pattern $\mathcal{T}^{*(8)}_{D_4}$, we may now turn to its twelvefold symmetric counterpart $\mathcal{T}^{*(12)}_{D_4}$ (the pattern $\mathcal{T}^{(12)}_{D_4}$, which is the analogue of $\mathcal{T}^{(8)}_{D_4}$, cf. Appendix B, is described in Appendix C). Here, we have to choose a different 'physical space' $\mathbb{E}_\|$ according to Eq. 3.7, wherefore the projection image $\pi_\perp(V(\mathbf{0}))$ changes to the regular dodecagon of Fig. 12. It is subdivided into elementary polygons that stem from the maximal intersection of 2-boundaries of $V(\mathbf{0})$. The latter can be grouped into four classes of triangles which form the prototiles of the pattern. Their possible arrangements around a vertex point of the tiling are — in complete analogy to Sec. 4 — in one-to-one correspondence to the elementary polygons that can be combined to 19 orbits w. r. t. the symmetry group d_{12}. The 19 representative vertex configurations are shown in Fig. 13; in Tab. 2 we give their relative frequencies in an infinite pattern which is defined by

$$\mathcal{T}^{*(12)}_{D_4}(\mathbf{c}_\perp) = \{\pi_\|(P^*) \ \mid\ P \in \mathcal{V}^{(2)}, \quad \mathbf{c}_\perp \in \pi_\perp(P)\} \tag{5.1}$$

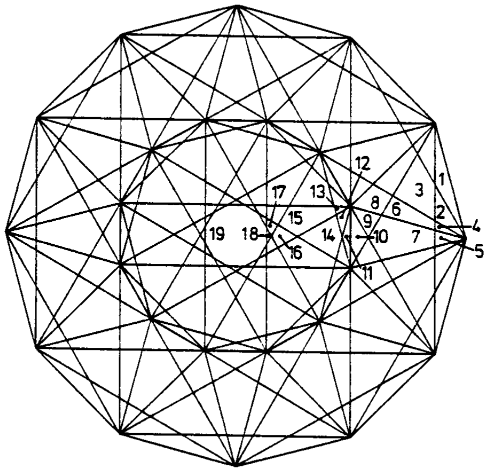

Figure 12: Projection image of the Voronoi cell in $\mathbb{E}_\perp$with twelvefold symmetry. The numbering of the elementary polygons corresponds to the numbering of vertex configurations in Fig. 13.

where $\mathbf{c}_\perp$ has to obey the same restrictions as in the previous section in order to avoid singular tilings. A finite patch of a generic tiling is shown in Fig. 4, a diffraction plot of delta scatterers at the vertex positions,

$$\{\pi_\|(\mathbf{q}) \ | \ \mathbf{q} \in D_4, \quad \mathbf{c}_\perp - \pi_\perp(\mathbf{q}) \in \pi_\perp(V(\mathbf{0}))\} \tag{5.2}$$

in Fig. 14. The latter was calculated along the lines presented in Sec. 4, the difference between the exact determination of the kinematic factor and its approximation by the Bessel function being even smaller than in the previous example.

The discussion of the local deflation properties of the twelvefold pattern is with the exception of one additional feature quite similar to that of the eightfold case. Like in the eightfold case we have a linear 4-D transformation which leaves the lattice invariant and acts on $\mathbb{E}_\|$ and $\mathbb{E}_\perp$ seperately. But this time it is not only a contraction and dilation of the two subspaces, because it incorporates also rotations by $\pi/12$ in $\mathbb{E}_\|$ and $5\pi/12$ in $\mathbb{E}_\perp$

$$M = \sqrt{\rho} \begin{pmatrix} c & -s \\ s & c \end{pmatrix} \pi_\| + \frac{1}{\sqrt{\rho}} \begin{pmatrix} c' & -s' \\ s' & c' \end{pmatrix} \pi_\perp, \tag{5.3}$$

where $\rho = 2 + \sqrt{3}$ is the so-called platinum number [23],

$$\begin{aligned} c := \cos(\gamma), \ s := \sin(\gamma), \\ c' := \cos(5\gamma), \ s' := \sin(5\gamma), \end{aligned} \tag{5.4}$$

and $\gamma = \pi/12$.

M acts as a global transformation on the pattern. But like in Sec. 4 it is possible to find a local transformation which only makes reference to a small neighbourhood of the considered point. Fig. 13 shows the deflation of the vertex configurations with the necessary extensions into the neighbourhood. Together with the prescription that in the center of every big equilateral triangle one has to draw a deflated small equilateral one (cf. Fig. 13), the deflation is now uniquely determined. If one aplies the deflation twice one will end up with the usual kind of transformation according to Sec. 4.

There exists also a local inflation rule but again we leave out the details here.

Let us close this Section with a short comment on the relationship of the presented pattern to the twelvefold pattern in [25]. It is easy to see that there exists a local transformation rule

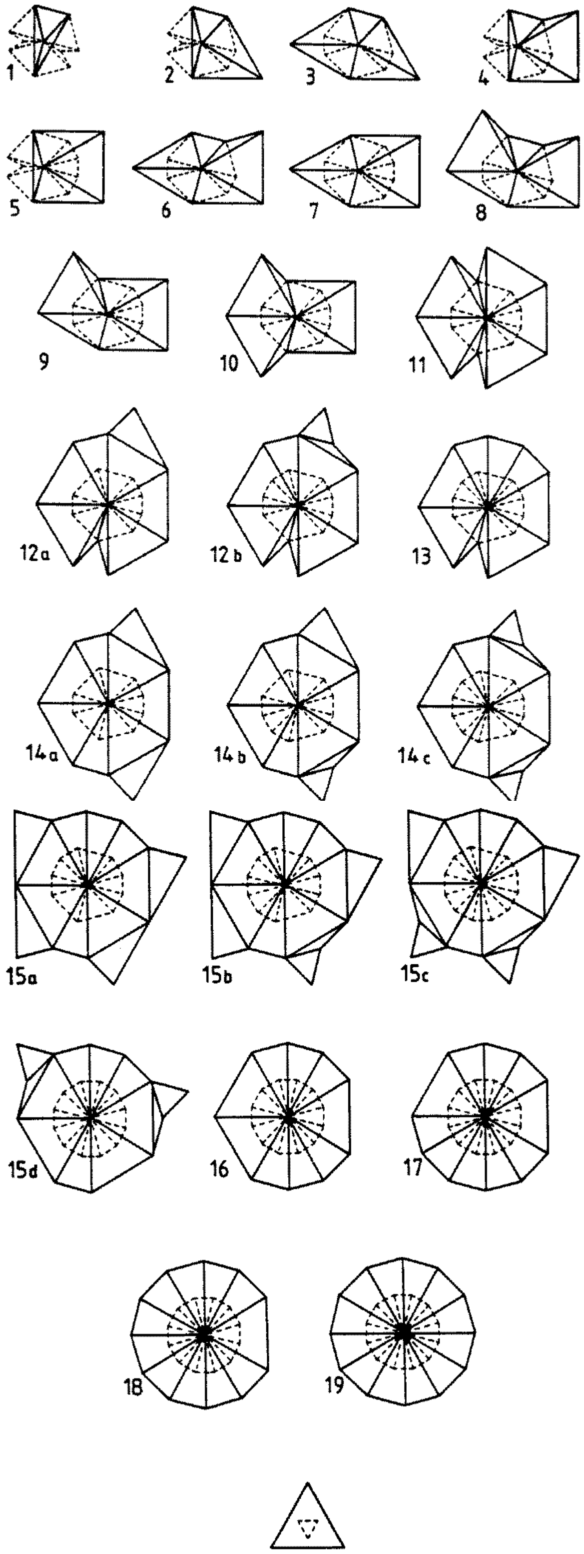

Figure 13: Vertex configurations of $\mathcal{T}_{D_4}^{*(12)}$ and their deflation. Some non-uniquely deflated vertices appear in two or more variations; their deflation is controlled by the immediate neighbourhood. The single triangle at the bottom of the picture indicates the deflation rule of the centre of the large equilateral triangle.

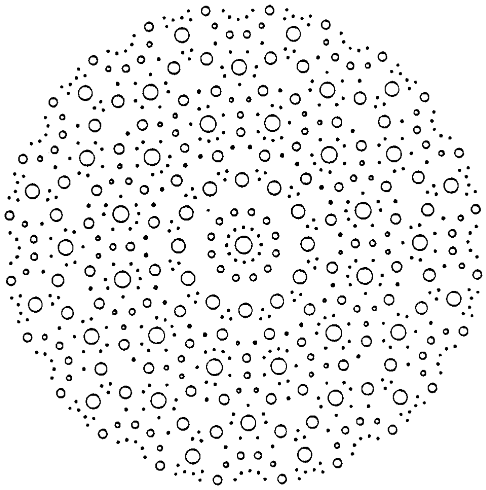

Figure 14: Calculated diffraction image of delta scatterers at vertex positions of $\mathcal{T}^{*(12)}_{D_4}$.

from the D_4 pattern to that in [25]. From the construction algorithm in [25] we can prove that there exists no local prescription the other way round. We have not systematically investigated the relationship to other twelvefold symmetric patterns [13] but preliminary results indicate that most of them belong to different classes w. r. t. mutual local derivability.

6 Conclusion

Although quite a few quasiperiodic tilings of the plane with eight- or twelvefold symmetry are known [13], we have presented two new examples each. Our physical motivation was the coexistence of octagonal and dodecagonal phases in $V_{15}Ni_{10}Si$ which calls for a unified description by an embedding into the same higher-dimensional lattice. For the quasiperiodic part, this is possible by means of the root lattice D_4 and we have analyzed this scenario. The transition between the phases requires a single parameter that can be seen as a rotation in 4-space. It may be chosen in such a way that during the transition fourfold symmetry is maintained — a phenomenon which has recently been observed in a slightly different context [22] of octagonal quasicrystals.

The continuation to periodic phases is also possible which raises, e. g., the question for an approach to possible phase transition via the phenomenologic Landau Theory [26]. To this end, one should extend the embedding to obtain a 'real' 3-D phase first which can be done by going from D_4 to $D_4 \otimes \alpha\mathbb{Z}$ or to D_6 [9]. This would also enable a systematic investigation of the existence of zone axes with almost or pseudo symmetry, as done recently for the decagonal quasiperiodic T–phase [27]. However, this is beyond the scope of the present article and we hope to tackle some of these questions in the near future.

7 Acknowledgement

This work is part of a study on the structure and properties of quasicrystals done at Tübingen University. We are grateful to our colleagues, in particular to P. Kramer, for helpful discussions and fruitful comments. Financial support from Deutsche Forschungsgemeinschaft and Alfried Krupp von Bohlen und Halbach Stiftung is gratefully acknowledged.

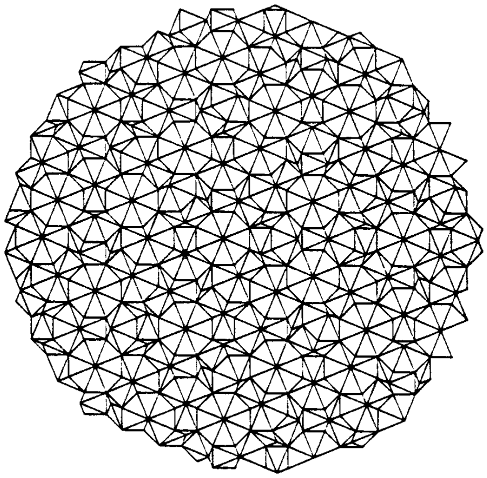

Figure 15: Pattern $\mathcal{T}^{(8)}_{D_4}$. The tiles are projection images of Voronoi 2-boundaries.

8 Appendix A — Minimal embedding of non-crystallographic symmetries for quasicrystals

Non-crystallographic symmetry groups play an important role in the description of quasicrystals, in particular for the determination of the higher-dimensional, periodic embeddings. In the corresponding 'hyperspace', the symmetry is compatible with the translational invariance which is broken by the so-called 'physical space' that appears as a suitably chosen section through the hyperspace.

Now, minimal embedding is required to avoid, e.g., unnecessary ambiguities for the generalized Miller indices. However, this is not yet sufficient; one has to demand additionally that the symmetry under investigation should faithfully operate in the physical space, not only in hyperspace. For the icosahedral group Y_h, this requires $D = 6$ where the $\mathbb{Q}$ -irreducible 6-D representation splits into two $\mathbb{R}$-irreducible 3-D inequivalent representations that operate faithfully on the 3-D physical space and the 3-D complementary or perpendicular space [24]. The 4-D irrep of Y_h also is compatible with a lattice (e.g., with the root lattice A_4), but does not allow any invariant subspace of dimension less than 4 — thus this irrep is not suitable for the construction of icosahedrally symmetric structures in 3-space.

A similar situation can be met with the embedding of the cyclic group C_n, either as a pure rotation or as a transformation with negative determinant. This question has been solved completely in terms of so-called additive versions of Euler's totient (or Phi-) function [28, 29], however without the additional restriction to the quasicrystalline situation. Here, one is interested in the minimal embedding of C_n by pure rotations in such a way that there is at least one 2-D subspace on which C_n acts faithfully, i.e., as an n-fold rotation. Following the referee's comments of [29] one can readily modify the argument for the present needs. A necessary condition for an orthogonal transformation T of order n to be compatible with translational symmetry is

$$P(x) = \det(T - x\mathbb{1}) = \sum_{j=1}^{N} m_j x^j \qquad (m_j \in \mathbb{Z}), \tag{8.1}$$

i.e., its characteristic polynomial has integer coefficients only. The eigenvalues of T are n-th roots of unity, and hence

$$P(x) \;\mid\; (x^n - 1)^r \tag{8.2}$$

for some $r \in \mathbb{N}$. Since the ring $\mathbb{Q}[x]$ of polynomials is factorial, we may assume $r = 1$ without loss of generality. A standard result of algebra [30] tells us

$$(x^n - 1) = \prod_{d|n} Q_d(x) \tag{8.3}$$

where the $Q_d(x)$ are the cyclotomic polynomials,

$$Q_d(x) = \prod_{(k,d)=1, 1\le k\le n-1} (x-\xi^k), \qquad \xi = \exp(\frac{2\pi i}{d}) \tag{8.4}$$

These polynomials are irreducible over $\mathbb{Q}$ (and thus over $\mathbb{Z}$), possess integer coefficients only, and are of degree $\phi(d)$, where $\phi(m)$ denotes Euler's Phi function:

$$\begin{aligned} \phi(p^k) &= p^k - p^{k-1} \qquad \text{for } k \in \mathbb{N} \text{ and } p \text{ prime} \\ \phi(m_1 m_2) &= \phi(m_1)\cdot\phi(m_2) \qquad \text{for coprime integers } m_1,\, m_2. \end{aligned} \tag{8.5}$$

Here, one can rederive the result of [28, 29] and also its 'quasicrystalline version'. To construct a quasiperiodic pattern with n-fold symmetry, we need the 2-D plane and a faithful, $\mathbb{R}$-irreducible representation of C_n. Amongst the eigenvalues of T we therefore must find at least one primitive n-th root of unity. Since $Q_n(x)$ is $\mathbb{Q}$-irreducible, there is no way out: we must have

$$Q_n(x) \mid P(x) \tag{8.6}$$

and hence $\deg(P(x)) \geq \deg(Q_n(x)) = \phi(n)$. On the other hand, nothing more than $Q_n(x)$ is necessary which can be shown starting from the regular representation of C_n in the primitive hypercubic lattice $\mathbb{Z}^n$ following standard arguments [23]. This gives also a constructive algorithm to explicitly find lattices of dimension $\phi(n)$ that provide the minimal embedding.

Thus we have the result that minimal embedding of C_n for the needs of quasicrystallography leads to lattices of dimension $\phi(n)$. Let us give an example for the difference to the ordinary crystallographic scenario: C_{15} can act as a lattice transformation in a 6-D lattice (e.g., one could take the root lattice $A_2 \otimes A_4$), but there is no 2-D subspace with a faithful operation of C_{15}. To find the latter, we have to climb up to $D = 8 = \phi(15)$. Since $\phi(m) = \phi(2m)$ for m odd, we automatically find an embedding of C_{30}. The analogous property holds for all C_n with n odd.

9 Appendix B

In this Appendix, we very briefly present the second canonical choice of an eightfold symmetric pattern that can be derived from D_4 and is denoted by $\mathcal{T}^{(8)}_{D_4}$. Here, the 2-boundaries of the Voronoi complex of D_4 are the preimages of the tiles in $\mathbb{E}_{\|}$ while the Delaunay complex is projected to $\mathbb{E}_{\perp}$ for the geometric analysis of the pattern. It is built from the same three triangular prototiles as $\mathcal{T}^{*(8)}_{D_4}$ and is shown in Fig. 15 for a generic shift vector $\mathbf{c}_{\perp}$, the general notation and geometric scenario being that of Sec. 4. Here, $\mathbf{c}_{\perp}$ for a generic pattern is restricted in such a way that it must not lie in the projection image of any 1-boundary of the Delaunay complex. As a consequence, we cannot produce the pattern around a point of global eightfold symmetry. Nevertheless, it will have generalized d_8 symmetry, i.e., the transformed patterns are in the same local isomorphism class. The analysis of vertices can be performed in analogy to Sec. 4. One would find 11 vertices mod. d_8 that split into 2 classes due to their relation to the 2 representative Delaunay cells. With respect to translations alone, we could distinguish between 4 classes of vertices.

10 Appendix C

Like in the eightfold case, the lattice D_4 also for the twelvefold case yields a second canonical tiling, called $\mathcal{T}^{(12)}_{D_4}$, by interchanging the roles of the Voronoi and the Delaunay complex. If we project

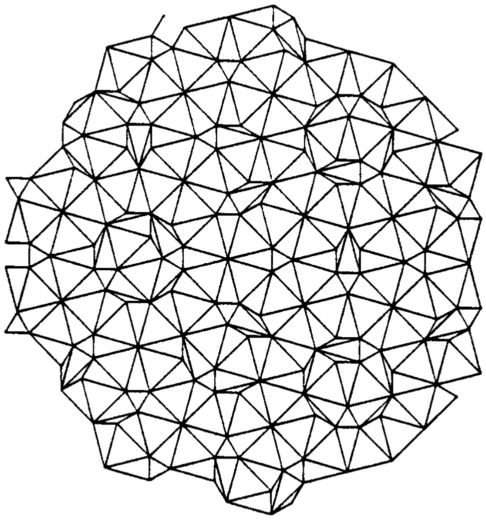

Figure 16: Pattern $\mathcal{T}_{D_4}^{(12)}$. The tiles are projection images of Voronoi 2-boundaries.

2-boundaries of the Voronoi complex to $\mathbb{E}_{\|}$ according to the dualization scheme, we obtain Fig. 16 for a pattern with generic shift vector $\mathbf{c}_{\perp}$. Again, $\mathbf{c}_{\perp}$ must not lie in the projection image of any 1-boundary of the Delaunay complex. Like in Appendix B, it is, under these conditions, impossible to produce a generic pattern around a point of global twelvefold symmetry. Nevertheless, the pattern has generalized point symmetry d_{12} because the action of any d_{12} operation transforms the pattern into a locally isomorphic one. It is funny to observe that this pattern is built from the same four triangular prototiles as its partner $\mathcal{T}_{D_4}^{*(12)}$ described in Sec. 5. The vertex analysis yields 8 vertex configurations mod. d_{12} that split into 4 classes w. r. t. T_{D_4} translations according to the 4 representative Delaunay cells. However, they are in a single orbit w. r. t. $T_{D_4} \otimes_s d_{12}$. Like in Appendix B, we will omit details here for the sake of brevity, more information is available from the authors on request.

References

[1] L. Bendersky *Phys. Rev. Let.* **55** (1985) 1461

[2] N. Wang, H. Chen, and K. H. Kuo, *Phys. Rev. Let.* **59** (1987) 1010

[3] T. Ishimasa, Y. Fukano, and H.-U. Nissen, *Phys. Rev. Let.* **55** (1985) 511
T. Ishimasa, H.-U. Nissen, and Y. Fukano *Phil. Mag.* **A 58** (1988) 835

[4] H. Chen, D. X. Li, and K. H. Kuo, *Phys. Rev. Let.* **60** (1988) 1645

[5] W. Steurer, *Zeitschrift f. Kristallographie* **190** (1990) 179

[6] M. Baake, P. Kramer, M. Schlottmann, and D. Zeidler, *Mod. Phys. Let.* **B 4** (1990) 249 and *Int. J. Mod. Phys.* **B 4** (1990) 2217

[7] M. Baake, D. Joseph, P. Kramer, and M. Schlottmann, *J. Phys.* **A 23** (1990) L1037

[8] M. Baake, M. Schlottmann, and P. D. Jarvis, preprint TPT-QC-90-11-1

[9] P. Kramer, Z. Papadopolos, and D. Zeidler, preprint TPT-QC-90-10-1

[10] N. D. Mermin, D. S. Rokhsar, and D. C. Wright *Phys. Rev. Let.* **58** (1987) 2099

[11] H. Brown, R. Bülow, J. Neubüser, H. Wondratschek, and H. Zassenhaus, "Crystallographic Groups in Four-Dimensional Space", (Wiley, New York, 1978)

[12] J. H. Conway, and N. J. A. Sloane, "Sphere Packings, Lattices and Groups", (Springer, New York, 1988)

[13] F. Gähler, in "Quasicrystalline Materials", ed. C. Janot and J. M. Dubois, (World Scientific, Singapore, 1988)

J. E. S. Socolar, *Phys. Rev.* **B 39**, (1989) 10519

H.-U. Nissen, in "Quasicrystals, Networks, and Molecules of Fivefold Symmetry", ed. I. Hargittai, (VCH, New York, 1990)

P. Stampfli, loc. cit.

[14] P. Kramer and M. Schlottmann, *J. Phys.* **A 22**, (1989) L1097

[15] P. Kramer, *Acta Cryst.* **A 43**, (1987) 486

[16] H. S. M. Coxeter, L. Few, and C. A. Rogers, *Mathematica* **6** (1959) 147

[17] F. P. M. Beenker, Eindhoven, TH-Report 82-WSK-04 (1982)

Z. M. Wang and K. H. Kuo, *Acta Cryst.* **A 44**, (1988) 857

[18] M. Baake, B. Gemünden, and R. Oedingen, *J. Math. Phys.* **23**, (1982) 944, *J. Math. Phys.* **23** (1982) 2595, *J. Math. Phys.* **24**, (1983) 1021,

[19] J. L. Birman and L.-C. Chen, *J. Math. Phys.* **12** (1971) 2454

[20] H. S. M. Coxeter, "Regular Polytopes", (Dover, New York, 1973)

[21] M. Baake and D. Joseph, *Phys. Rev.* **B 42** (1990) 8091

[22] K. H. Kuo, in "Proceedings of the Anniversary Adriatico Research Conference on Quasicrystals, ICTP, Trieste, Italy, 1989", ed. M. V. Jaric and S. Lundqvist, (World Scientific, Singapore, 1990)

[23] K. Niizeki, *J. Phys.* **A 22** (1989) 193

[24] P. Kramer, *Mod. Phys. Let.* **B 1** (1987) 7, *Int. J. Mod. Phys.* **B 1** (1987) 145, *J. Math. Phys.* **29** (1988) 516

[25] J.-F. Sadoc and R. Mosseri, *J. Phys. France* **51** (1990) 205

[26] J.-C. Toledano and P. Toledano, "The Landau Theory of Phase Transitions", (World Scientific, Singapore, 1989)

[27] A. Knupfer and P. Kramer, preprint TPT-QC-90-12-1

[28] C. Hermann, *Acta Cryst.* **2** (1949) 139

[29] H. Hiller, *Acta Cryst.* **A 41** (1985) 541

[30] S. Lang, "Algebra", (Addison-Wesley, Menlo Park, 1984)

Table 1:

No. of vertex	rel. frequency	approx. value in %
1	$5 - 2\lambda$	17.16
2	$-24 + 10\lambda$	14.21
3	$17 - 7\lambda$	10.05
4	$58 - 24\lambda$	5.89
5	$-65 + 27\lambda$	18.38
6	$-41 + 17\lambda$	4.16
7	$58 - 24\lambda$	5.89
8	$17 - 7\lambda$	10.05
9	$-140 + 58\lambda$	2.44
10	$99 - 41\lambda$	1.72
11	$99 - 41\lambda$	1.72
12	$-41 + 17\lambda$	4.16
13	$-70 + 29\lambda$	1.22
14	$29 - 12\lambda$	2.94

Table. 1 The relative frequencies of the vertices of $\mathcal{T}^{*(8)}_{D_4}$ (cf. Fig. 1), $\lambda = 1 + \sqrt{2}$ is the silver number.

Table 2:

No. of vertex	rel. frequency	approx. value in %
1	$15 - 4\rho$	7.18
2	$\frac{2}{3}(-26 + 7\rho)$	8.29
3	$\frac{1}{3}(19 - 5\rho)$	11.32
4	$\frac{2}{3}(-97 + 26\rho)$	2.22
5	$56 - 15\rho$	1.92
6	$\frac{4}{3}(71 - 19\rho)$	12.14
7	$\frac{1}{3}(-272 + 73\rho)$	14.66
8	$-41 + 11\rho$	5.26
9	$\frac{2}{3}(71 - 19\rho)$	6.07
10	$\frac{1}{3}(-26 + 7\rho)$	4.15
11	$56 - 15\rho$	1.92
12	$-306 + 82\rho$	2.82
13	$209 - 56\rho$	0.52
14	$224 - 60\rho$	7.70
15	$-138 + 37\rho$	8.59
16	$\frac{2}{3}(-97 + 26\rho)$	2.22
17	$\frac{1}{3}(265 - 71\rho)$	0.81
18	$\frac{1}{3}(-362 + 97\rho)$	0.30
19	$56 - 15\rho$	1.92

Table. 2 The relative frequencies of the vertices of $\mathcal{T}_{D_4}^{*(12)}$ (cf. Fig. 4), $\rho = 2 + \sqrt{3}$ is the platinum number.